A Robust Controller Design based on Kharitonov's Theorem for Frequency Control in an Interconnected Power System

Beheshteh Raouf and Seyedamirabbas Mousavian

***Abstract* — The load frequency control of power systems is often carried out using methods that are dependent on the system load and parameters. Therefore, the controller design is not robust in unforeseen cases such an attack on the power system, variations in system parameters, or changes in load. In such methods, there is a need for an attack detection tool, and moreover, the controller parameters need to be adjusted as the load and power system parameters change. In this paper, Kharitonov's theorem was applied to design a robust decentralized load frequency control for a two-area power system in the presence of electric vehicle fleets as a power source that were targeted by a cyberattack. Furthermore, the robustness of the system against system nonlinearities was demonstrated by testing the efficacy of the controller on both linear and nonlinear systems. The controller design was robust such that there was no need to change the gains of the controller even during an attack. This was compared with the performance of controllers designed using GWO algorithm and fuzzy logic that needed retuning for different case studies with different variations in system parameters, load, or inclusion of a cyberattack to the electric vehicle fleets.**

***Keywords* — Electrical Vehicles (EVs), Load Frequency Control (LFC), Kharitonov's Theorem.**

I. Introduction

Continuous supply of electric power with good quality to all power system consumers is a top priority for power system stakeholders. Satisfying the power quality requirements requires a balance between the power demand and the power generated. A significant frequency deviation caused by an attack or unexpected event may lead to serious instability, huge economic losses, or even a power system collapse [1]. Hence, automatic voltage regulation and load frequency control (LFC) are used to balance the reactive and real power balance, respectively [2]. The LFC is intended to monitor the system frequency and tie-line power of the control areas to keep their frequency at or close to acceptable values [3].

Multi-area power systems have interconnected control areas, as often is the case in the real world. Each control area has multiple sources of electricity generation with different mix of conventional energy sources such as thermal, gas, and nuclear units, as well as renewable energy sources (RES) such as solar and wind [4]. Moreover, recently EVs are shown to have great potential for use as renewable energy storage [5]. The bidirectional flow of energy provided by the vehicle to grid (V2G) technology enables the EVs to act as an energy source [6]. This promising technology strengthens the renewable energy sources adaption [7] and creates numerous benefits such as grid stability, peak load management, power quality [8] and cost-saving for market participants [9]. In V2G, the EVs work as energy routers that transfer the energy from charging stations powered by renewable energy sources (RES) and other sources to the power grid. Through routing the energy, the extra generation may be stored in EVs battery to be applied when required, which lowers the energy waste as well.

However, the use of advanced technologies such as V2G makes the power systems more prone to security threats [10], [11]. Generally, an attacker may target either the cyber layer or the physical components in the power systems. The former targets the power systems by manipulating the integrity of measurement data or denial of service (DoS) by obstructing communications. The latter, which was considered in this paper, takes place when an attacker manipulates the system parameters and generation capacity causing fluctuations in frequency, which can damage system components. Failure in security of the power system puts its stability and economic operation at risk. Therefore, it is crucial to develop control methods that are more secure against disturbances, can mitigate consequences of attacks, and can maintain system stability during unexpected operational periods.

A comprehensive study on potential attacks to the LFC systems is presented in [12], which highlights the importance of considering EVs in the security of the LFC systems. Many investigations of attacks on LFC systems are focused on attack detection [13] or attack modeling and its impact on system dynamic performance [14] rather than designing a controller to mitigate the attacks.

Several controller design methods have been proposed to calculate the proportional-integral (PI) or proportional integral derivative (PID) controller parameters. The application of various soft computing algorithms such as the salp swarm algorithm [15] and GWO [16] have been utilized in the literature to optimize the controller parameters. Combined intelligent techniques have also been proposed for LFC [3]. The success of these techniques requires an accurate selection of input and output scaling factors of the controller and is highly dependent on the designer's experience. Moreover, these techniques are not always robust under disturbances and variations in the operation of the system.

Submitted on November 07, 2022.
Published on January 13, 2023.
B. Raouf, Department of Electrical and Computer Engineering, Clarkson University, Potsdam, New York, USA.
(corresponding e-mail: raoufb@clarkson.edu)
S. Mousavian, Engineering and Management Program, Clarkson University, Potsdam, New York, USA.
(e-mail: smousavi@clarkson.edu)

Several LFC studies have shown acceptable results using adaptive control technique [17], [18]. However, adaptive control needs accurate real time data of the system, which limits its application in real power systems.

To overcome the limitations, various robust control techniques are proposed. Sliding mode controller [19], model predictive control [20], have been proposed to design a robust load frequency system against the system uncertainties and disturbances. However, these techniques often have difficult mathematical computations and are usually suitable for the nominal model of system. This makes using them in the controller design for real-time systems with uncertain interval models, in which the parameters of the system can vary, challenging.

In contrast, Kharitonov's theorem is a robust yet simple controller design approach for such power systems. In this method, variations of the system parameters are considered during the design of PI or PID controllers [21]. Kharitonov's theorem has been used to study different problems in power systems such as the reactive power control [22] and load frequency control [23], [24]. However, these studies do not consider robustness of the system against an attack to the power system.

This paper demonstrates robustness of controller design using Kharitonov's method for LFC of an interconnected multi-area power system with EVs as a power source that are targeted by a cyberattack. Furthermore, robustness of this controller design against system nonlinearities, not included in controller design, are shown. The effectiveness and robustness of LFC based on Kharitonov's theorem is illustrated by comparing its performance to controllers designed using fuzzy logic and GWO algorithm for linear and nonlinear systems. Robustness of LFC based on Kharitonov's theorem allowed using the same controller parameters independent of the system or load variations in contrast to GWO [25] or fuzzy logic methods that needed readjustment of the controller parameters.

The rest of the paper is organized as follows. The Kharitonov's theorem is discussed in Section II, subsection A. The details of the two-area power system model used here is described in Section II, subsection B. The interval model of each power generating unit of the system is presented in Section II, subsection C, followed by the stability analysis in Section II, subsection D. The robust controller design using Kharitonov's theorem is discussed in Section II, subsection E. The robust performance of the Kharitonov controller for linear and nonlinear systems is compared with the fuzzy logic and the GWO algorithm in Section F.

II. Methods

A. Kharitonov theorem

In this paper, Kharitonov's theorem was used to design a robust controller for a power system with varying parameters. The power system was composed of thermal, hydro, gas generation units, and EV fleets. A linear mathematical model of this system was used. The first step in applying Kharitonov theorem is to define an interval polynomial set ρ, given in (1)-(3).

$$\rho \triangleq p(s,Q) = q_0 + q_1 s + \cdots + q_n s^n \quad (1)$$

$$q_i \subset Q, q_i \in [q_i^-, q_i^+] \quad (2)$$

$$q_i^-, q_i^+ \in R, \forall i = 0, \cdots, n \;\; q_i^- \leq q_i^+ and q_i^-, q_i^+ \neq 0 \quad (3)$$

According to Kharitonov's theorem, only four special polynomials are required to determine the stability of all polynomials of the system. These four special Kharitonov polynomials can be computed considering lower and upper bounds, ($i.e.$, q_i^- and q_i^+). In general, Kharitonov polynomials are [21] (4)-(7).

$$K_1(s) = q_0^- + q_1^- s + q_2^+ s^2 + q_3^+ s^3 + q_4^- s^4 \quad (4)$$

$$K_2(s) = q_0^- + q_1^+ s + q_2^+ s^2 + q_3^- s^3 + q_4^- s^4 \quad (5)$$

$$K_3(s) = q_0^+ + q_1^- s + q_2^- s^2 + q_3^+ s^3 + q_4^+ s^4 \quad (6)$$

$$K_4(s) = q_0^+ + q_1^+ s + q_2^- s^2 + q_3^- s^3 + q_4^+ s^4 \quad (7)$$

Equations (4)-(7) form the vertices of Kharitonov's rectangle for a given s. To apply this method to the system under study, the mathematical model of the system should be obtained. The model of the power plant is described as $G(s)$, given by (8).

$$G(s) = \frac{[a^-, a^+]}{p(s,Q)} a^-, a^+ \in R \quad (8)$$

Based on Kharitonov's theorem "the system is robustly stable if and only if the four Kharitonov polynomials are stable" [21]. Considering the numerator and denominator of $G(s)$ ($i.e.$ K_1 to K_4), eight models are obtained. Next, the stability of these eight models must be analyzed. Here, to determine the stability, Routh-Hurwitz stability criterion and the zero-inclusion principle were employed. After ensuring stability, the PI controller is designed.

To study the stability of the system based on Kharitonov's theorem, the characteristic polynomial of the closed loop system, $\Delta(s)$, is needed, which is defined as (9).

$$\Delta(s) = 1 + C(s)G(s) \quad (9)$$

where $G(s)$ is the plant model defined as (10).

$$G(s) = \frac{N(s)}{D(s)} \quad (10)$$

and $C(s)$ is the PID controller given in (11).

$$C(s) = K_P + \frac{K_I}{s} + K_D s \quad (11)$$

Substituting $s = j\omega$, where $j^2 = -1$ and ω is the angular frequency, $C(s)$ and $G(s)$ can be written in the frequency domain. Then splitting $N(s)$ and $D(s)$ into their odd and even parts, Ne, No, De, and Do, and assuming $K_D = 0$, $C(s)$ and $G(s)$ can be written as (12) and (13).

$$G(j\omega) = \frac{N_e(-\omega^2) + j\omega N_o(-\omega^2)}{D_e(-\omega^2) + j\omega D_o(-\omega^2)} \quad (12)$$

$$C(j\omega) = K_P + \frac{K_I}{j\omega} \quad (13)$$

Substituting $G(j\omega)$ and $C(j\omega)$ in (7) and decomposing the result into its even and odd parts, $\Delta(s)$ can be written as (14).

$$\Delta(j\omega) = [K_I N_e(-\omega)^2 - \omega^2 K_P N_o(-\omega)^2 - \omega^2 D_o(-\omega^2)] + j[\omega K_P N_e(-\omega^2) + \omega K_I N_o(-\omega^2) + \omega D_e(-\omega^2)] \quad (14)$$

To extract the K_P and K_I parameters, we need to separate the real and imaginary parts of $\Delta(j\omega)$ and equate them to zero which yields (15) and (16).

$$K_I N_e(-\omega^2) - \omega^2 K_P N_o(-\omega^2) = \omega^2 D_o(-\omega^2) \quad (15)$$

$$\omega K_P N_e(-\omega^2) + \omega K_I N_o(-\omega^2) = \omega D_e(-\omega^2) \quad (16)$$

Equation (15) and (16) provide a relationship between K_P and K_I for a fixed K_D as a function of ω. Next, we used the stability boundary locus method to determine the proper values of K_P and K_I that would make the system stable [23; 26]. In this method, the $\psi(K_P, K_I)$ plane is divided into stable and unstable regions. This method ensures the stability of the various plants described by $G(s)$ in equation 6 by identifying the best values for K_P and K_I.

B. System model for LFC

We selected a two-area power system with multiple sources to better show the performance of the designed controller. The two-area power system included thermal, hydro, and gas generation units, as well and the EV fleets, as illustrated in Fig. 1. There are three input types in each area including the controller inputs, U_T, U_G, U_H and U_E; the load disturbances ΔP_{D1} and ΔP_{D2}; and the incremental change in tie-line power ΔP_{tie}. The outputs are the system frequency deviations Δf_1 and Δf_2 and the area control errors, ACE_1 and ACE_2. The area control errors are given by (17).

$$ACE_i = B_i \Delta f_i + \Delta P_{tie}, \; i = 1,2 \quad (17)$$

where B_1 and B_2 are the frequency bias parameters of the first and second area, respectively.

In Fig. 1, R_T, R_H and R_G are constant droop coefficients for thermal, hydro, and gas units, respectively and all were taken to be $R = 2.4$ p.u.MW/Hz. $TD = 5\ s$ is the time delay. The time constants for speed governor and steam turbine of the thermal power plant are $T_G = 0.08s$ and $T_t = 0.3s$ respectively.$T_r = 10s$ and $K_r = 0.3$ are the steam turbine reheat constants.

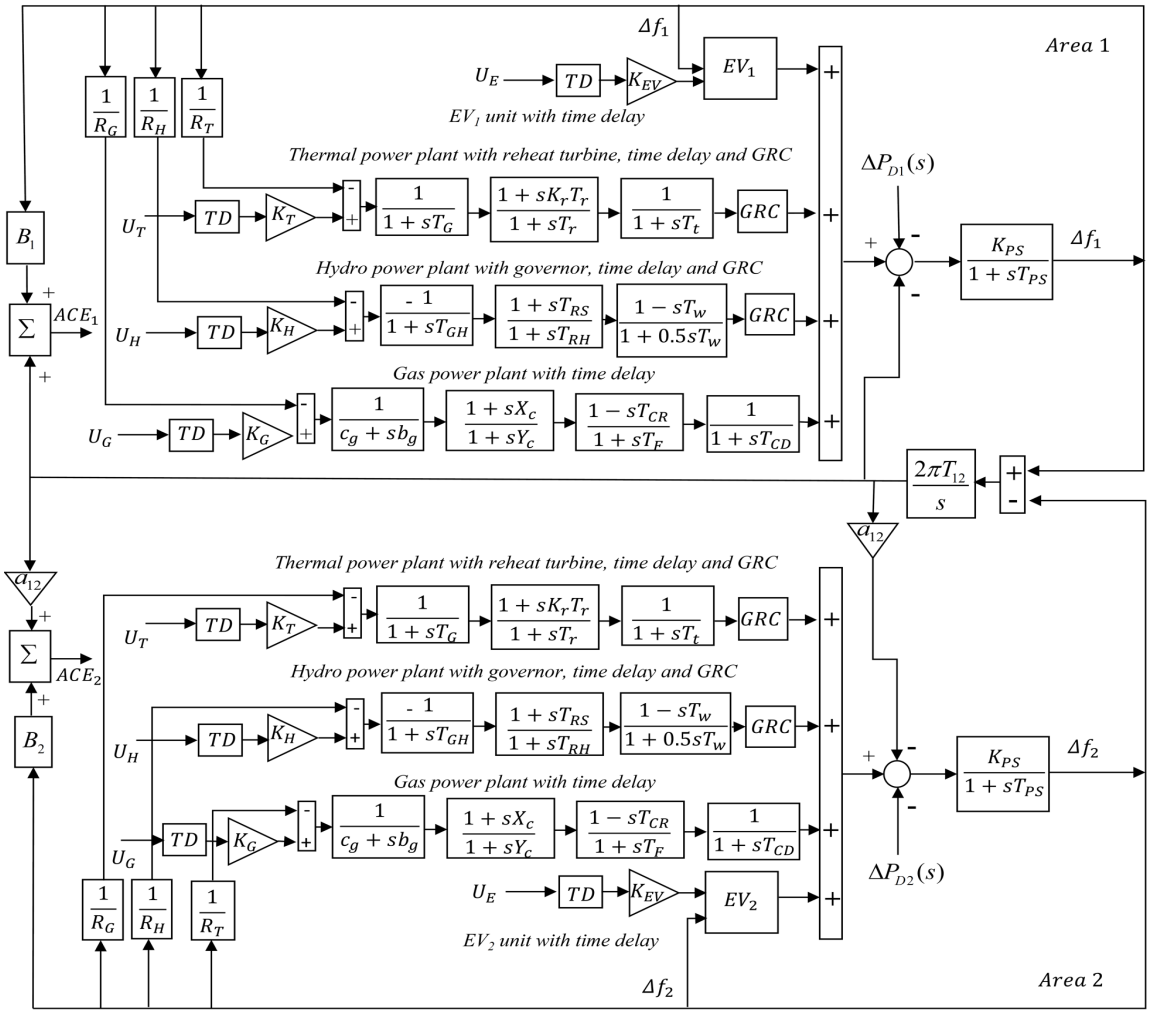

Fig. 1. Model of two-area power system including thermal, gas, hydro and EVs units.

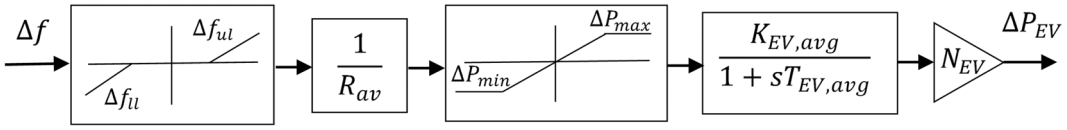

Fig. 2. The structure of EV_1 and EV_2 models.

The generation rate constraint is denoted as $GRC = 0.05$. For the hydro power plant, $T_{GH} = 0.2s$ is the time constant for the turbine speed governor main servo. $T_{RS} = 5s$ is the hydro turbine speed governor reset time and $T_{RH} = 28.75s$ is the transient droop time constant for the turbine speed governor. $T_w = 1$ s is the nominal starting time of water in the penstock. For the gas power plant $c_g = 1$ and $b_g = 0.05$ are the gas turbine valve positioner and its constant. $X_c = 1$ and $Y_c = 1s$ are the lead and lag time constants of the gas turbine speed governor.

$T_F = 0.23s$ is the fuel time constant and $T_{CR} = 0.01s$ is the combustion reaction time delay of the gas turbine. $T_{CD} = 0.2s$ is the gas turbine compressor discharge volume time constant. $K_{PS} = 68.96$ and $T_{PS} = 11.49s$ are the power system gain and time constant respectively. $T_{12} = 0.0433$ is the tie line power coefficient. The participation factors of thermal, hydro, gas and EV generating units are respectively denoted by $K_T = 0.7$, $K_H = 0.1$, $K_G = 0.15$, and $K_{EV} = 0.05$.

In general, the participation factor of generating units determines the contribution of the units to the nominal load. The optimal value of the participation factor of each generating unit depends on a variety of factors such as generation capacity, availability, generation costs, and efficiency of the unit [27], [28]. For example, gas turbine units can respond to variations in load quickly. Therefore, they are ideal for periods of peak demand or periods of highly varying loads whereas EVs generation may not be quickly available during sudden increases in demand. Considering that the V2G is a promising technology and relatively new, we considered 5% participation factor for EVs in this study. The EVs could play a bigger role when there is higher volatility in the system, $e.g.$ when renewable sources of energy have a higher participation factor in the electricity generation mix.

The structure of EV_1 and EV_2 models in Fig. 1 was based on [29] and is illustrated in Fig. 2. The first limit in Fig. 2 is the dead-band for the frequency ranging from $\Delta f_{ll} = -0.01$ to $\Delta f_{ul} = 0.01$. R_{av} is the droop coefficient for EVs and was set to $1Hz/p.u.MW$. The second limit is $\Delta P_{min} = -3kW$ to $\Delta P_{max} = 3kW$, which are the minimum and maximum of EV fleets output and is known as the regulation capacity. $K_{EV,avg} = 1s$ and $T_{EV,avg} = 1s$ are the average participation factor and the time constant in the EV transfer function, respectively. N_{EVs} is the number of the EVs, which was set to 1000 units for each area. ΔP_{EV} is the incremental generation change of EV.

The transfer functions of thermal, hydro and gas power units, respectively $G_T(s)$, $G_H(s)$ and $G_G(s)$, considering the droop characteristics is (18).

$$\frac{G_p(s)G_t(s)G_g(s)}{1+\frac{G_p(s)G_t(s)G_g(s)}{R}} \tag{18}$$

where $G_P(s)$ represents the transfer function of load and machine dynamics and is a common part of thermal, hydro and gas units given in (19).

$$G_P(s) = \frac{K_{PS}}{1+sT_{PS}} \tag{19}$$

and $G_t(s)$ and $G_g(s)$ are different for each unit and determine the dynamics of turbine and governor, respectively. For the transfer function of the thermal unit $G_T(s)$, (20) is used.

$$G_g(s) = \frac{1}{1+sT_G};\ G_t(s) = \frac{K_rT_rs+1}{1+(T_rs)(1+T_ts)} \tag{20}$$

For the transfer function of the hydro unit $G_H(s)$, (21) is used.

$$G_g(s) = \frac{1}{1+sT_{GH}};\ G_t(s) = \frac{(1-sT_W)(1+sT_{RS})}{(1+0.5T_Ws)(1+T_{RH}s)} \tag{21}$$

and for the transfer function of the gas unit $G_G(s)$, (22) is used.

$$G_g(s) = \frac{1+sX_G}{1+sY_G};G_t(s) = \frac{1-sT_{CR}}{(c_g+sb_g)(1+sT_F)(1+sT_{CD})} \tag{22}$$

For the EVs the transfer function, (23) is used.

$$G_{EV}(s) = \frac{G_p(s)G_e(s)}{1+\frac{G_p(s)G_e(s)}{R_{av}}} \tag{23}$$

where (24) is used for calculating $G_e(s)$.

$$G_e(s) = \frac{1}{1+sT_{EV,avg}} \tag{24}$$

Note that nonlinearities in the system including the generation rate constraints, GRC, and time delays TD were neglected to simplify the controller design. These nonlinear effects were considered as an additional source of system variation against which the robustness of the Kharitonov's controller was assessed.

C. Numerical Analysis

In this study, all the parameters of the generating units were varied ± 50 % within their nominal values. This was done to design a robust controller where uncertainties in the actual power system are already considered during the design. For instance, substituting (20) in (18) yields the transfer function of thermal unit given in (25)-(27).

$$G_T = \frac{N_T}{D_T} \quad (25)$$

$$N_T = (K_{PS}K_rT_r)s + K_{PS} \quad (26)$$

$$D_T = T_GT_rT_tT_{PS}s^4 + (T_rT_tTPS + T_GT_tT_{PS} + T_GT_tT_r + T_GT_{PS}T_r)s^3 + (T_GT_r + T_tT_{PS} + T_tT_r + T_{PS}T_r + T_tT_G + T_{PS}T_G)s^2 + \left(T_G + T_r + T_t + T_{PS} + \frac{K_rK_TK_{PS}T_r}{R}\right)s + 1 + \frac{K_TK_{PS}}{R} \quad (27)$$

Replacing each parameter in (26) and (27) with its numerical range gives transfer function for each unit shown in (28) and (29).

$$N_T(s) = [25.85,698]s + [34.47,103] \quad (28)$$

$$D_T(s) = [0.17,13.96]s^4 + [5.52,149]s^3 + [30.77,276]s^2 + [32.48,226]s + 29.73 \quad (29)$$

The denominator of $G_T(s)$ gives the following Kharitonov polynomials for thermal units.

$$K_{T1}(s) = 0.17s^4 + 149s^3 + 276s^2 + 32.48s + 29.73$$
$$K_{T2}(s) = 0.17s^4 + 5.52s^3 + 276s^2 + 226.74s + 29.73$$
$$K_{T3}(s) = 13.96s^4 + 149s^3 + 30.77s^2 + 32.48s + 29.73$$
$$K_{T4}(s) = 13.96s^4 + 5.52s^3 + 30.77s^2 + 226s + 29.73 \quad (30)$$

The associated Kharitonov polynomials for hydro, gas units and EV fleets are calculated (31)-(33).

$$K_{H1}(s) = 2.06s^4 + 794s^3 + 483s^2 + 77.93s + 29.73$$
$$K_{H2}(s) = 2.06s^4 + 29.405s^3 + 483s^2 + 233s + 29.73$$
$$K_{H3}(s) = 167s^4 + 794s^3 + 53.73s^2 + 77.93s + 29.73$$
$$K_{H4}(s) = 167s^4 + 29.40s^3 + 53.73s^2 + 233s + 29.73 \quad (31)$$

$$K_{G1}(s) = 0.05s^4 + 22.33s^3 + 44.7s^2 + 11.98s + 29.23$$
$$K_{G2}(s) = 0.05s^4 + 0.76s^3 + 44.7s^2 + 53.82s + 29.23$$
$$K_{G3}(s) = 4.07s^4 + 22.33s^3 + 3.72s^2 + 11.98s + 30.23$$
$$K_{G4}(s) = 4.07s^4 + 0.76s^3 + 3.72s^2 + 53.82s + 30.23 \quad (32)$$

$$K_{E1}(s) = 25.8525s^2 + 6.245s + 15.3659$$
$$K_{E2}(s) = 25.8525s^2 + 18.735s + 15.3659$$
$$K_{E3}(s) = 2.8725s^2 + 6.245s + 43.0978$$
$$K_{E4}(s) = 2.8725s^2 + 18.735s + 43.0978 \quad (33)$$

D. The Stability Tests

The stability of each individual unit was investigated since an unstable unit may put the stability of the entire system at risk. A ± 50 % variation of the nominal value for unit parameters which are subject to perturbations was considered. The Routh-Hurwitz stability criterion test and zero inclusion principle, which are two well-known stability tests of Kharitonov's theorem, were applied.

The Routh-Hurwitz matrix for Kharitonov polynomials was computed using the H matrix. The stability of polynomials was then determined based on the sign of the elements in the matrix [30]. Except for the EV fleets, which had no right-side poles, other generating units had at least two right-side poles that could make them unstable.

The zero-inclusion principal test was applied by identifying Kharitonov rectangles for each unit and determining whether they included the origin or not. Kharitonov polynomials form the vertices of Kharitonov's rectangle. The edges of these rectangles are parallel to the imaginary and real axes. In the case of $p(j\omega, Q)$, when ω increases from 0 to ∞, the size, and aspect ratio of the sides of rectangle change. These sets of rectangles are named" moving boxes". In this stability test, none of the boxes should include the origin for the system to be stable [31].

Fig. 3 shows the moving boxes for the thermal units. The zero-inclusion principle is violated, which indicates potential system instability. Similarly, the moving boxes for the hydro and gas units included the origin. On the other hand, the origin was outside the moving boxes for the EV fleets, confirming their stability. Therefore, the overall system is unstable for some ranges of frequency, which necessitates developing a robust controller.

E. Robust Controller Design Using Kharitonov's Theorem

To address the system instability, a decentralized controller was designed for frequency control of the two-area and multi-source power system illustrated in Fig. 1. The controller design approach based on Kharitonov's theorem for a single area power system is described in Section II-A. In the case of the two-area power system shown in Fig. 1, the local feedback control was achieved through the multiplication of bias parameters B_1 and B_2 with the transfer function of (16) [32]. This allowed modeling each area independently. To design the decentralized controller, the ΔP_T was assumed to be zero [33].

In the case of the thermal units, the local feedback control was achieved through (32).

$$G_T(s) = B_i\frac{N_T(s)}{D_T(s)} \quad ,i = 1,2 \quad (34)$$

The nominator of $G_T(s)$ is a first-order equation with two parameters K_{PS} and T_r. The denominator defines the four Kharitonov polynomials that must pass the stability analysis tests mentioned in section II-D. According to the complex equation given for the numerators, to find the value for the K_P and K_I that provides stability, a family of 16 sets of loci was required for each of thermal, hydro and gas units. The numerator of EV fleets was not a complex function and only 8 sets were required. Replacing sets loci for each unit into (7), and then substituting s with $j\omega$ and separating the imaginary and real parts would result in K_P and K_I as functions of ω. K_P and K_I functions for thermal units were (35) and (36).

$$K_p(w) = \frac{n_{p1}\omega^4 + n_{p2}\omega^2 + n_{p3}}{d_{p1}\omega^2 + d_{p2}} \quad (35)$$

$$K_I(w) = \frac{n_{I1}\omega^4 + n_{I2}\omega^2 + n_{I3}}{d_{I1}\omega^2 + d_{I2}} \quad (36)$$

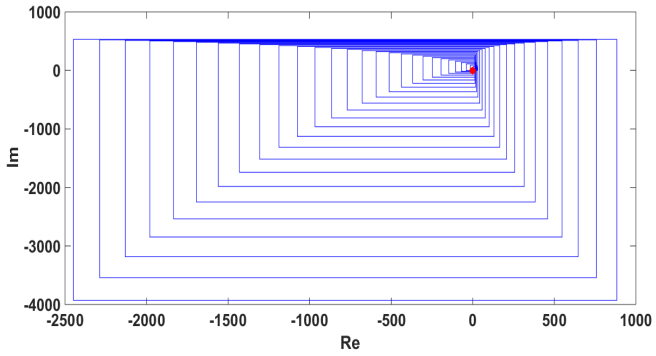

Fig. 3. Kharitonov's rectangle corresponding to thermal units.

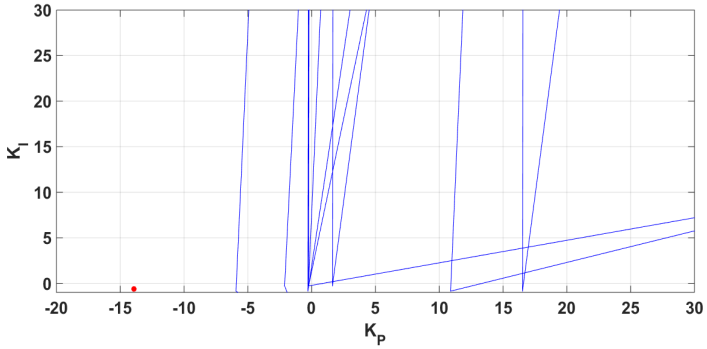

Fig. 4. The location of PI controller parameters in $K_P - K_I$ plane for thermal unit.

The 32 calculated functions for K_P and K_I for thermal units are plotted in $K_P - K_I$ plane for a range of ω varying from 0 to 10 kHz. Based on Kharitonov' s theorem, the value of the controller parameter should be located between the common space of these lines and the horizontal axis. For example, in Fig. 4 the values for K_P and K_I were selected from the common region shared by all loci and the $K_I = 0$ which is illustrated with a red point. The best value of (K_P and K_I) obtained for thermal units in Fig. 4 was found after tens of simulation studies as $(-13.9, -0.64)$. Then, for each pair K_P and K_I values, the K_D value was optimized based on tens of more simulations. The best values of (K_P , K_I and K_D) for the Kharitonov controller are given in Table I.

F. PID Controller Design using Fuzzy Logic and GWO Algorithm

The performance of the PI controller designed based on the Kharitonov' s theorem in terms of frequency deviation and incremental change in tie-line power were then compared with PID controllers tuned by pure fuzzy logic and GWO algorithm. The objective function, J, of the GWO algorithm [25] is given in (37).

$$J = \sqrt{J_1^2 + J_2^2}$$
$$J_i = \int_0^t (|\Delta f_i| + |\Delta P_{tie}|)^2 dt\,, \qquad i = 1,2 \tag{37}$$

subject to the constraints of (38).

$$-50 \le K_P, K_I, K_D \le 50 \tag{38}$$

The pure fuzzy logic was performed in Simulink® using the fuzzy logic toolbox. The membership functions and fuzzy logic rules applied are shown in Fig. 5 and Table II, respectively.

The effectiveness of the designed Kharitonov controller was tested using three sensitivity analysis scenarios: 1) Changes in the load, 2) Changes in the load and a cyberattack through disconnection of EVs, 3) Changes in the load and variation in the value of some of the key system parameters. In the first scenario, we assumed a 1% and 2% increase in the load of the first and second areas respectively. The PID controller parameters optimized by fuzzy logic and the GWO algorithm for the first scenario are given in Table I.

For fuzzy logic and the GWO algorithms, the PID controller parameters were tuned again for each scenario. The controller designed using Kharitonov's method was kept fixed in all three scenarios.

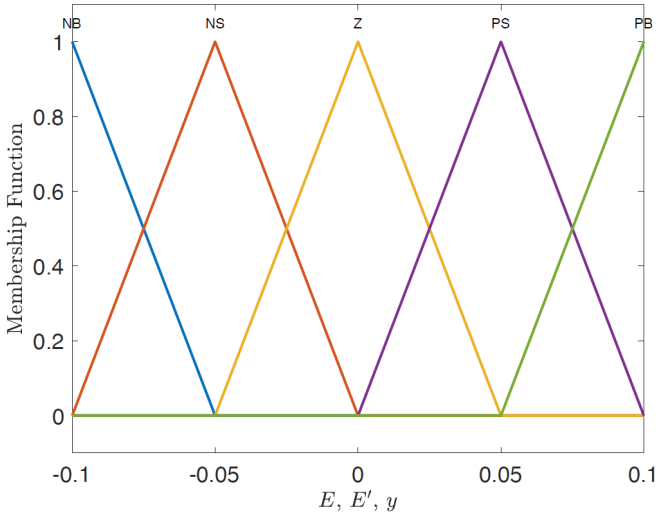

Fig. 5. Membership function for error, derivative of error and controller output.

TABLE I: CONTROLLER PARAMETERS FOR KHARITONOV'S THEOREM (IN ALL SCENARIOS), FUZZY LOGIC AND GWO ALGORITHM (IN THE FIRST SCENARIO)

Technique	Unit	K_P	K_I	K_D
Kharitonov	Thermal	-13.9	-0.64	-3.87
	Gas	-16.5	-5.1	3.56
	Hydro	26.3	-1.2	3.56
	EV	5.5	0.68	1
Fuzzy	Thermal	6.36	-5.12	-12.32
	Gas	-20	-4.58	-3.50
	Hydro	-16.74	-0.01	-7.18
	EV	11.38	4.29	9.84
GWO	Thermal	-17.26	7.49	-0.78
	Gas	-14.54	-16.29	-6.64
	Hydro	-19.86	-0.37	-9.42
	EV	8.85	5.63	6.34

TABLE II: RULE BASE USED IN FUZZY LOGIC FOR ERROR, DERIVATIVE OF ERROR AND CONTROLLER OUTPUT

E / E'	NH	NL	Z	PL	PH
NH	NH	NH	NH	NL	Z
NL	NH	NL	NL	Z	PH
Z	NH	NL	Z	PL	PH
PL	NH	Z	PL	PH	PH
PH	Z	PL	PH	PH	PH

TABLE III: THE SENSITIVITY ANALYSIS OF SYSTEM

	Δf_1			Δf_2			Δf_3		
	$T_s(s)$	Overshoot	Undershoot	$T_s(s)$	Overshoot	Undershoot	$T_s(s)$	Overshoot	Undershoot
					First scenario				
Kharitonov	5.51	440×10^{-6}	-22.71×10^{-3}	3.47	6.75×10^{-3}	-50.65×10^{-3}	28.27	7.16×10^{-3}	$-204\times \mathbf{10^{-6}}$
Fuzzy	23.98	2.34×10^{-3}	-17.37×10^{-3}	18.14	4.97×10^{-3}	-41.21×10^{-3}	24.91	5.83×10^{-3}	$-882\times \mathbf{10^{-6}}$
GWO	24.20	2.6×10^{-3}	-17.22×10^{-3}	21.41	5.35×10^{-3}	-41.19×10^{-3}	26.64	5.7×10^{-3}	$-1.12\times \mathbf{10^{-3}}$
					Second scenario				
Kharitonov	27.83	0.0064	-0.0974	35.51	0.0039	-0.0779	39.17	4.5039×10^{-4}	-0.0076
Fuzzy	20.17	0.005	-0.1236	29.64	0.0044	-0.1255	41.47	4.3102×10^{-4}	-0.0064
GWO	19.54	0.0046	-0.1251	18.40	0.0041	-0.1267	41.06	4.31×10^{-4}	-0.0064
					Third scenario				
Kharitonov	5.74	409×10^{-6}	-22.12×10^{-3}	3.18	6.38×10^{-3}	-49.91×10^{-3}	27.41	6.95×10^{-3}	$-190.53\times \mathbf{10^{-6}}$
Fuzzy	17.13	1.97×10^{-3}	-20.03×10^{-3}	10.80	7.17×10^{-3}	-40.90×10^{-3}	18.40	5.37×10^{-3}	$-691.62\times \mathbf{10^{-6}}$
GWO	20.80	$26.77\times \mathbf{10^{-6}}$	$-19.28\times \mathbf{10^{-3}}$	7.36	$4.15\times \mathbf{10^{-3}}$	$-40.90\times \mathbf{10^{-3}}$	10.58	$5.43\times \mathbf{10^{-3}}$	0

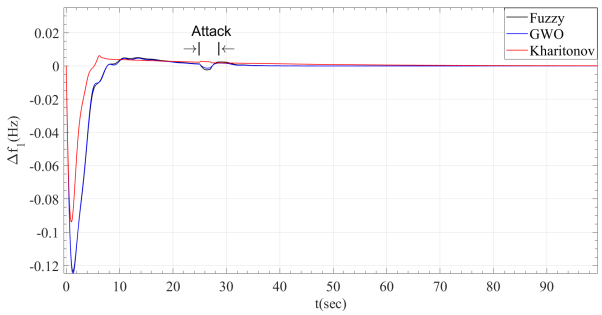

Fig. 6. Frequency response of the first area for load increase and disconnection of EV fleets.

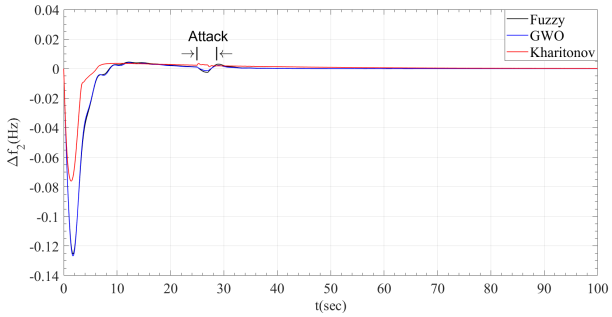

Fig. 7. Frequency response of the second area for load increase and disconnection of EV fleets.

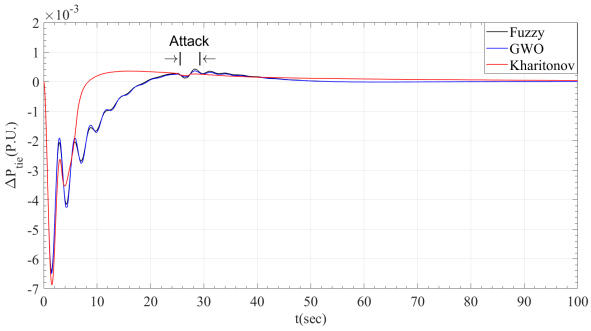

Fig. 8. Tie line deviation for load increase and disconnection of EV fleets.

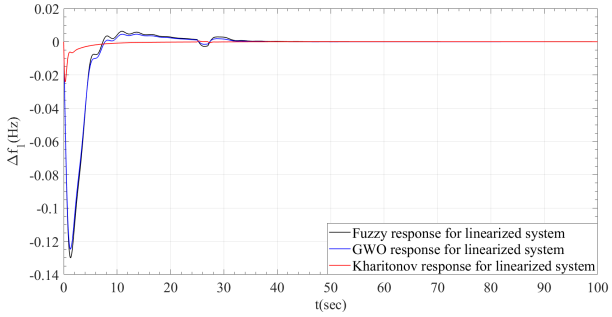

Fig. 9. Comparison of frequency deviation of the first area between three methods without physical constraints consideration

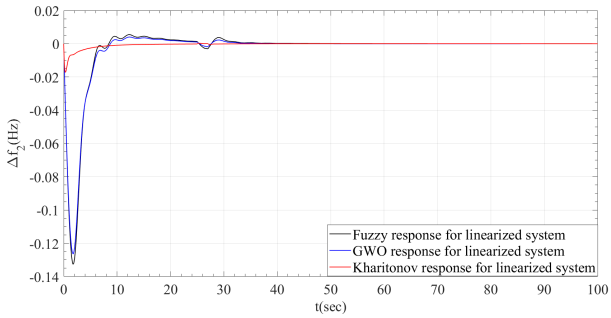

Fig. 10. Comparison of frequency deviation of the second area between three methods without physical constraints consideration.

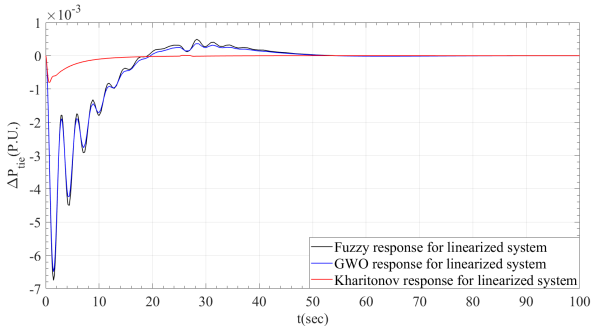

Fig. 11. Comparison of tie-line power deviation between three methods without physical constraints consideration.

There was no need to readjust the controller parameters for different loading conditions or variations in system parameters since these were considered during the controller design. The numerical values corresponding to settling time (T_s), overshoot, and undershoot for all three scenarios are given in Table III. The settling time was measured as the time when the deviation between the system response and the steady-state response reduced below 2% of maximum deviation. The average value of settling times of Δf_1, Δf_2 and ΔP_{Tie} was 12.42 seconds for the Kharitonov controller. This was, respectively, 44.4% and 47% faster than the average settling time of controllers designed using the fuzzy logic and the GWO algorithm, demonstrating the effectiveness of the Kharitonov controller in damping the oscillations quickly. Additionally, the value of overshoot in Δf_1 was much smaller for the Kharitonov controller compared to the other two techniques.

The second scenario evaluated the performance of the designed controller when the system faced an attack. It was assumed that the attacker can manipulate the EV fleets connection to the power grid during the peak demand. In this scenario, respectively, 3% and 2% increases in the load of

the first and second areas was assumed. Furthermore, it was assumed that the attacker disconnects the EV fleets connection at $t = 25\ s$ while the other three units continued to serve the load. This attack was modeled as a decrease in the participation factor of EV fleets to 0 at $t = 25\ s$ for 2 seconds. The frequency of the first and second area and tie-line deviations are shown in Fig. 6-8, respectively and the numerical results are given in Table III. The attack caused a jump in the frequency and the tie-line power. Although the controller parameters were retuned for GWO algorithm and fuzzy logic methods, they showed inferior performance compared to the Kharitonov controller. Also, there are more oscillations in the frequency and tie line power deviations for the GWO algorithm and the fuzzy logic compared to Kharitonov controller, which could have adverse effects on power system components.

In the third scenario, the load change was the same as the first one ($i.e.$ 1% increase in the load of the first area and a 2% increase in the load of the second area). Additionally, $\pm 20\%$ change in the speed governor time constant of the thermal unit, T_G, and the gas turbine compressor discharge volume time constant, T_{CD} was assumed. This scenario examined the robustness of Kharitonov' s theorem by varying system parameters. The numerical results are given in Table III. The average settling time of Kharitonov' s theorem, $i.e.$, 12 seconds, is 7.7% faster than that of the GWO algorithm and 20% faster than that of the fuzzy logic method. Thus, considering the variations of the parameters during the controller design using Kharitonov' s theorem, reduced the system sensitivity to variations in system parameters. Although the nonlinearities due to generation rate constraints and time delays were neglected in design of the Kharitonov's controller, the results of previous three scenarios illustrated that the designed Kharitonov controller performed robustly for the nonlinear system under changes in load, cyberattack and variation in system parameters. To assess the performance of the system for a linear system, the nonlinearities in the system including generation rate constraints and time delays were eliminated and the performance of the designed controller in terms of the frequency and tie-line power deviations for this linear system was evaluated for the second scenario where a change in load was accompanied by a cyberattack. The results shown in Fig. 9-11 show that the Kharitonov controller had a better performance in terms of controlling settling times compared to controllers designed using GWO algorithm and fuzzy logic. Note that the GWO and the fuzzy logic controllers were retuned for the linear system. Moreover, even though the LFC performed better on the linear system in terms of settling time, overshoot and undershoot, it was very effective for the nonlinear system as well.

III. Conclusion

The Kharitonov's theorem was used to design a robust load frequency controller for a two-area multi-source power system including a fleet of electric vehicles as a power source. The performance of the controller designed based on the Kharitonov's theorem was evaluated under three scenarios including load variations, system parameter variations, and an attack on the communication of EV fleets. The effects of time delay and generation time constraints were considered as additional sources of system variation in all three scenarios.

In comparison of the performance of the controller designed based on Kharitonov's theorem with controllers designed based on GWO and fuzzy logic, the robustness of design based on Kharitonov's theorem was demonstrated. Whereas controller parameters needed to be tuned again for each scenario using GWO or fuzzy logic algorithms, the same controller designed with Kharitonov's theorem performed well under all three scenarios. The comparison approved the efficacy of the Kharitonov controller, particularly in terms of settling time and damping the oscillations into the appropriate range.

Additionally, there was no need to change the controller parameters even for large disturbances or an attack. Finally, the performance of the Kharitonov controller along with fuzzy logic and GWO controllers for the linearized system was demonstrated for the second scenario, which included a cyberattack. This showed the role of nonlinearities in the system. Although the controller was designed for a linear system, it worked well under conditions where nonlinearities were present in the system. This demonstrated the robustness of the simplified Kharitonov controller designed for the linearized system against nonlinear system variations.

References

[1] Li P, Wang X, Lee WJ, Xu D. Dynamic power conditioning method of microgrid via adaptive inverse control. *IEEE Transactions on power delivery,* 2015 Jan 14;30(2):906-13.
[2] Kundur PS, Malik OP. Power system stability and control. *McGraw-Hill Education;* 2022.
[3] Aziz S, Wang H, Liu Y, Peng J, Jiang H. Variable universe fuzzy logic-based hybrid LFC control with real-time implementation. *IEEE Access.* 2019 Feb 28;7:25535-46.
[4] Kothari DP, Nagrath IJ. Modern power system analysis *Tata McGraw*.
[5] Debbarma S, Dutta A. Utilizing electric vehicles for LFC in restructured power systems using fractional order controller. *IEEE transactions on smart grid,* 2016 Mar 1;8(6):2554-64.
[6] Khokhar B, Dahiya S, Parmar KP. Load Frequency Control of a Multi-Microgrid System Incorporating Electric Vehicles. *Electric Power Components and Systems,* 2022 Mar 5:1-7.
[7] Geetha TS, Amudha V, Chellaswamy C. A Novel Dynamic Capacity Expansion Framework Includes Renewable Energy Sources for an Electric Vehicle Charging Station. *International Transactions on Electrical Energy Systems,* 2022 Sep 10;2022.
[8] Justin F, Peter G, Stonier AA, Ganji V. Power quality improvement for vehicle-to-grid and grid-to-vehicle technology in a microgrid. *International Transactions on Electrical Energy Systems,* 2022; 2022.
[9] Kazemi MA, Sedighizadeh M, Mirzaei MJ, Homaee O. Optimal siting and sizing of distribution system operator owned EV parking lots. *Applied energy,* 2016 Oct 1;179:1176-84.
[10] Raouf B, Mousavian S, Ghazinour K. Interconnected and Complex Electric Power and Transportation Systems: a SWOT Analysis. *Current Sustainable/Renewable Energy Reports,* 2021 Sep 8:1-5.
[11] Kumari A, Trivedi M, Tanwar S, Sharma G, Sharma R. SV2G-ET: A Secure Vehicle-to-Grid Energy Trading Scheme Using Deep Reinforcement Learning. *International Transactions on Electrical Energy Systems,* 2022 Apr 29;2022.
[12] Mohan AM, Meskin N, Mehrjerdi H. A comprehensive review of the cyber-attacks and cyber-security on load frequency control of power systems. *Energies,* 2020 Jul 28;13(15):3860.
[13] Chen C, Zhang K, Yuan K, Zhu L, Qian M. Novel detection scheme design considering cyber attacks on load frequency control. *IEEE Transactions on Industrial Informatics,* 2017 Oct 23;14(5):1932-41.
[14] Liu S, Liu XP, El Saddik A. Denial-of-Service (dos) attacks on load frequency control in smart grids. *In2013 ieee pes innovative smart grid technologies conference (isgt),* 2013 Feb 24 (pp. 1-6). IEEE.
[15] Hasanien HM, El-Fergany AA. Salp swarm algorithm-based optimal load frequency control of hybrid renewable power systems with

communication delay and excitation cross-coupling effect. *Electric Power Systems Research,* 2019 Nov 1;176:105938.

[16] Guha D, Roy PK, Banerjee S. Load frequency control of interconnected power system using grey wolf optimization. *Swarm and Evolutionary computation,* 2016 Apr 1;27:97-115.

[17] Elgammal A, Boodoo C. Optimal Hybrid Filtering Strategy Using Adaptive Genetic-Fuzzy Logic Control for Harmonics Reduction in a Standalone Micro Hydroelectric Power Plant Coordinated with a PV System. *European Journal of Electrical Engineering and Computer Science,* 2021 Aug 9;5(4):56-62.

[18] Rajesh KS, Dash SS. Load frequency control of autonomous power system using adaptive fuzzy based PID controller optimized on improved sine cosine algorithm. *Journal of Ambient Intelligence and Humanized Computing,* 2019 Jun;10(6):2361-73.

[19] Elgammal A, Ramlal T. Adaptive Voltage Regulation Control Strategy in a Stand-Alone Islanded DC Microgrid based on distributed Wind/Photovoltaic/Diesel/Energy Storage Hybrid Energy Conversion System. *European Journal of Electrical Engineering and Computer Science,* 2021 Jul 26;5(4):26-33.

[20] Liu J, Yao Q, Hu Y. Model predictive control for load frequency of hybrid power system with wind power and thermal power. *Energy,* 2019 Apr 1;172:555-65.

[21] Bhattacharyya SP, Keel LH. Robust control: the parametric approach. *In Advances in control education,* 1994-1995 Jan 1 (pp. 49-52). Pergamon.

[22] Raouf B, Akbarimajd A, Dejamkhooy A, SeyedShenava S. Robust distributed control of reactive power in a hybrid wind-diesel power system with STATCOM. *International Transactions on Electrical Energy Systems,* 2019 Apr;29(4):e2780.

[23] Saxena S, Hote YV. Decentralized PID load frequency control for perturbed multi-area power systems. *International Journal of Electrical Power & Energy Systems,* 2016 Oct 1;81:405-15.

[24] Lamba R, Singla SK, Sondhi S. Design of fractional order PID controller for load frequency control in perturbed two area interconnected system. *Electric Power Components and Systems,* 2019 Jul 21;47(11-12):998-1011.

[25] Mirjalili S, Mirjalili SM, Lewis A. Grey wolf optimizer. *Advances in engineering software,* 2014 Mar 1;69:46-61.

[26] Tan N, Kaya I, Yeroglu C, Atherton DP. Computation of stabilizing PI and PID controllers using the stability boundary locus. *Energy Conversion and management,* 2006 Nov 1;47(18-19):3045-58.

[27] Bevrani H. Robust power system frequency control. *New York: springer;* 2014 Jul.

[28] Mousavian S, Raouf B, Conejo AJ. Equilibria in Interdependent Natural-gas and Electric Power Markets: An Analytical Approach. *Journal of Modern Power Systems and Clean Energy,* 2021 Jul 30;9(4):776-87.

[29] Izadkhast S. Aggregation of plug-in electric vehicles in power systems for primary frequency control. Ph.D. dissertation, *Inst. Res.Technol., Comillas Pontifical Univ., Madrid, Spain,* 2017.

[30] Panneerselvam K, Ayyagari R. Computational complexity of Kharitonov's robust stability test. *International Journal of Control Science and Engineering,* 2013;3(3):81-5.

[31] Chapellat H, Bhattacharyya SP. A generalization of Kharitonov's theorem; Robust stability of interval plants. *IEEE transactions on automatic control,* 1989;34(3):306-11.

[32] Saxena S, Hote YV. Stabilization of perturbed system via IMC: An application to load frequency control. *Control Engineering Practice.* 2017 Jul 1;64:61-73.

[33] Tan W. Decentralized load frequency controller analysis and tuning for multi-area power systems. *Energy conversion and management,* 2011;52(5):2015-2023.